

Article

## Pre-Reduction of Au/Iron Oxide Catalyst for Low-Temperature Water-Gas Shift Reaction Below 150 °C

Shinji Kudo<sup>1,2</sup>, Taisuke Maki<sup>1</sup>, Takashi Fukuda<sup>1</sup> and Kazuhiro Mae<sup>1,\*</sup>

<sup>1</sup> Department of Chemical Engineering, Graduate School of Engineering, Kyoto University, Kyoto-daigaku Katsura, Nishikyo-ku, Kyoto 615-8510, Japan; E-Mails: shinji\_kudo@cm.kyushu-u.ac.jp (S.K.); tmaki@cheme.kyoto-u.ac.jp (T.M.); fukuda@cheme.kyoto-u.ac.jp (T.F.)

<sup>2</sup> Research and Education Center of Carbon Resources, Kyushu University, Kasuga 816-8580, Japan

\* Author to whom correspondence should be addressed; E-Mail: kaz@cheme.kyoto-u.ac.jp; Tel.: +81-75-383-2668; Fax: +81-75-383-2658.

Received: 6 October 2011; in revised form: 14 November 2011 / Accepted: 29 November 2011 / Published: 9 December 2011

---

**Abstract:** Low-temperature water-gas shift reaction (WGS) using gold catalyst is expected to be an attractive technique to realize an efficient on-site hydrogen production process. In this paper, Au/Fe<sub>3</sub>O<sub>4</sub> catalysts for promoting the WGS below 150 °C were developed by a preliminary reduction of Au/iron oxide (Fe<sup>3+</sup>) catalyst utilizing high reactivity of Au nano-particles. The reduction was conducted under a CO, H<sub>2</sub>, or CO/H<sub>2</sub>O stream at either 140 or 200 °C, and the effect of reduction conditions on the characteristics of the Au/Fe<sub>3</sub>O<sub>4</sub> catalyst and on the catalytic activity in WGS at 80 °C was investigated. The reaction progress during the pre-reduction treatment was qualitatively analyzed, and it was found that the iron oxide in Au/Fe<sub>2</sub>O<sub>3</sub> calcined at 200 °C was easily reduced to Fe<sub>3</sub>O<sub>4</sub> phase in all reduction conditions. The reduction conditions affected the characteristics of both Au and iron oxide, but all of the reduced catalysts had small Fe<sub>3</sub>O<sub>4</sub> particles of less than 20 nm with Au particles on the surface. The surface area and content of cationic Au were high in the order of CO, H<sub>2</sub>, CO/H<sub>2</sub>O, and 140, 200 °C. In the WGS test at 80 °C using the developed catalysts, the activities of the catalysts pre-reduced by CO at 140 or 200 °C and by H<sub>2</sub> at 140 °C were very high with 100% CO conversion even at such a low temperature. These results indicated that factors such as higher surface area, crystallized Fe<sub>3</sub>O<sub>4</sub>, and cationic Au content contributed to the catalytic activity.

**Keywords:** water-gas shift; gold catalyst; iron oxide; pretreatment; reduction; activation

---

## 1. Introduction

On-site hydrogen production from liquid fuels such as methanol and DME (dimethyl ether) is currently regarded as a promising technology for PEFC (Polymer electrolyte fuel cell) applications [1]. Methanol and DME are suitable for portable applications because of their high density and can be reformed to H<sub>2</sub> by catalytic steam reforming at relatively low temperatures. However, carbon monoxide and methane are also produced via side reactions such as decomposition reactions, reverse water-gas shift reaction, and methanation at high reaction temperatures above 300 °C. Because CO contained as by-product in the fuel poisons an electrode in the fuel cell [2], the on-site H<sub>2</sub> production process typically involves a series of reaction steps to remove CO after the reforming step, which is composed of water-gas shift reaction (WGS) and selective CO oxidation. In addition, methane has to be removed using pressure swing adsorption (PSA) with large energy consumption before supplying to PEFC. In this system, WGS is a key reaction that produces H<sub>2</sub> and CO<sub>2</sub> from H<sub>2</sub>O and CO, but is governed by thermodynamic equilibrium. Reducing CO requires the operation of the WGS at a low temperature. The present WGS process in on-site H<sub>2</sub> production system has adopted Cu/ZnO/Al<sub>2</sub>O<sub>3</sub> as a catalyst. The Cu-type catalyst is often used at temperatures in the range of 180–300 °C, but has little catalytic activity at lower temperatures, and the reactor is too big. Furthermore, the CO conversion is not more than 90% even using a good Cu-type catalyst due to chemical equilibrium restriction [3]. Thus, the development of catalysts to accelerate the reaction rate at low temperatures below 150 °C is desired to realize an efficient on-site H<sub>2</sub> production system.

Gold catalysts have been widely studied since the discovery of catalytically active nano-sized Au particles supported on metal oxides by Haruta *et al.* [4] This catalyst has an extremely high activity in CO oxidation reaction even at room temperature. In addition, gold catalysts on various metal oxides are highly active in many other reactions [5–13]. Andreeva *et al.* firstly applied the gold catalyst to the WGS and showed the potential for high catalytic activity even below 180 °C [14–16]. Among gold catalysts supported on various kinds of metal oxides, Au/Fe<sub>2</sub>O<sub>3</sub> is one of the active catalysts for low-temperature WGS due to the redox ability of Fe<sub>2</sub>O<sub>3</sub> [17]. In WGS, Fe<sub>2</sub>O<sub>3</sub> is easily reduced to the magnetite, Fe<sub>3</sub>O<sub>4</sub>, because it is the stable oxidation state in equilibrium [18] It is well known that Fe<sub>3</sub>O<sub>4</sub> is the catalytically active phase in high-temperature WGS, and this is applied to low-temperature WGS using gold-loaded iron oxide catalysts as well [19,20]. In these studies, the effect of Au/iron oxide catalysts was shown, but the state of catalyst structure was not strictly controlled because the reduction of Fe<sub>2</sub>O<sub>3</sub> and agglomeration of Au particles inevitably proceed during the reaction. If the Au particles remain as nano-particles on crystallized Fe<sub>3</sub>O<sub>4</sub> support with high surface area, it is expected that the reaction rate of WGS increases even below 150 °C, and a drastic CO reduction can be brought about with small reactor size.

To achieve this, the pre-reduction of Au/Fe<sub>2</sub>O<sub>3</sub> at low temperature is important because the porous structure of the iron oxide is easily destructured by heat. From this viewpoint, we first examined the WGS using catalysts prepared by different conditions, and then developed a proper pre-reduction

method to maintain small Au and Fe<sub>3</sub>O<sub>4</sub> nano-particles. Using these catalysts, the WGS reactivity at 80 °C was investigated, and the effect of the proposed pre-reduction method on the reduction of CO was clarified.

## 2. Experimental Section

### 2.1. Preparation of Au/Iron Oxide Catalysts

Au/iron oxide (Fe<sup>3+</sup>) catalyst was prepared from Fe(NO<sub>3</sub>)<sub>3</sub>·9H<sub>2</sub>O (Wako Pure Chemical Industries, Ltd.: Osaka, Japan) and HAuCl<sub>4</sub>·4H<sub>2</sub>O (Kojima Chemicals Co., Ltd.: Osaka, Japan) as precursor materials. The preparation method has been described in detail in our previous report [21]. The precursors were dissolved in distilled water to prepare 200 mL of 1.69–1.86 × 10<sup>2</sup> mmol L<sup>-1</sup> iron nitrate aqueous solution and 100 mL of 0.15–1.52 × 10 mmol L<sup>-1</sup> chlorauric acid aqueous solution for the synthesis of 3 g Au/iron oxide catalyst containing 1, 3, and 10 wt% Au. The pH value of the iron nitrate solution was controlled at 8.2 by adding Na<sub>2</sub>CO<sub>3</sub> powder (Wako Pure Chemical Industries, Ltd.: Osaka, Japan) for hydrolysis, and the suspension was vigorously stirred in a water bath at 60 °C. After 1 h of aging, the chlorauric acid solution was added to the iron hydroxide solution, followed by additional 0.5 h stirring. During the aging and mixing processes, the pH value was maintained within 8.0–8.4 by the addition of diluted nitric acid and sodium carbonate. The precipitates were filtered and washed with 1 L of distilled water (60 °C) to eliminate Cl<sup>-</sup> and Na<sup>+</sup>. Finally, they were vacuum-dried for 12 h at 80 °C, followed by calcination in a heater for 2 h at 200 or 400 °C. The prepared catalysts were sieved to the particle size between 0.3 and 1.0 mm for catalytic activity tests. Following is a summary of the catalysts prepared under different conditions: calcined at 200 °C with 1, 3, and 10 wt% Au and calcined at 400 °C with 3 wt% Au. In addition, iron oxide calcined at 200 °C with no Au content was also prepared by the same procedure as a reference. The catalysts, thus prepared, are collectively denoted as Au/Fe<sub>2</sub>O<sub>3</sub>, although the iron oxide might contain other oxidation states such as ferrihydrite, Fe<sub>5</sub>HO<sub>8</sub>·4H<sub>2</sub>O.

### 2.2. Catalyst Characterizations

X-ray diffraction (XRD) patterns of catalysts were measured by an X-ray diffractometer (RIGAKU, multiflex) equipped with a Cu-K $\alpha$  radiation source at a voltage of 40 kV and a current of 40 mA. The BET surface area and the pore size distribution were obtained from N<sub>2</sub> adsorption data at 77 K (BELJAPAN, Belsorp-mini) using the BET equation and the BJH method, respectively. The morphology and microstructure of catalysts were observed using a transmission electron microscope (TEM; JEOL, JEM-1010) at an accelerating voltage of 100 kV. For the TEM observations, samples were ground to fine powder and dispersed in ethanol using ultrasonic agitation. A drop of the suspension was then transferred to a carbon-coated Cu mesh grid and dried at room temperature. X-ray photoelectron spectroscopy (XPS) spectra were measured with SHIMADZU ESCA-3400 using an Al K $\alpha$  radiation source at an accelerating voltage of 10 kV and an emission current of 20 mA. The measurements were performed under vacuum pressure of less than 5 × 10<sup>-6</sup> Pa. A correction of binding energy was performed, referencing the position of C 1s peak at 284.8 eV.

### 2.3. Measurement of Catalytic Activity

Prepared catalysts were loaded into a quartz tube reactor with a 7 mm inner diameter for the catalytic activity test. The reaction temperature was controlled with an infrared gold image furnace by monitoring the temperature at inlet and outlet of the catalyst bed. Two kinds of WGS tests were conducted for examining catalytic activity: one is the temperature dependence test using as-prepared catalysts; and the other is the WGS at 80 °C using the samples reduced in various ways from Au/Fe<sub>2</sub>O<sub>3</sub> catalyst (Au: 3 wt%) calcined at 200 °C. In the temperature dependence test, the prepared Au/Fe<sub>2</sub>O<sub>3</sub> catalysts were used without pre-reduction. The catalyst bed was heated to the starting temperature, 140 °C, under an Ar stream and kept for 0.5 h to remove air and moisture, followed by the introduction of the reactant gas. The reactant gas (H<sub>2</sub> 45.9%, CO 8.3%, CO<sub>2</sub> 4.1%, H<sub>2</sub>O 41.7%) was fed to 0.4 g of the catalyst bed at gas hourly space velocity (GHSV) of 2600 h<sup>-1</sup>. In the WGS reaction test at 80 °C, the catalyst was reduced prior to the reaction. The pre-reduction was conducted under three different reducing gas streams, CO/N<sub>2</sub>, H<sub>2</sub>/Ar, and CO/H<sub>2</sub>O/N<sub>2</sub>, at two different temperatures, 140 and 200 °C. The flow rates of the reducing gases were 20, 20, and 26 (steam/carbon ratio, S/C = 10) mL min<sup>-1</sup>, respectively, over 0.3 g catalyst, where the flow rates of reducing gases, CO and H<sub>2</sub>, were unified to 0.62 mL min<sup>-1</sup>. After a 2 h pre-reduction, the temperature was decreased under an Ar stream to room temperature for characterizations of the reduced samples or to 80 °C for catalytic activity tests. In the WGS test at 80 °C, the reactant (CO/H<sub>2</sub>O/N<sub>2</sub> = 2.2/30.3/67.5) was introduced into the catalyst bed at GHSV = 2800 h<sup>-1</sup>. Since the partial pressure of H<sub>2</sub>O, about 30 kPa, is sufficiently lower than the saturation vapor pressure at 80 °C, 47.4 kPa, the vapor was not condensed to liquid.

The effluent gas from the reactor was diverted through a cold trap to remove H<sub>2</sub>O, mixed with an Ar flow of 50 mL min<sup>-1</sup> for dilution, and then analyzed using an on-stream gas chromatograph (VARIAN, CP-4900 Micro-GC) equipped with a thermal conductivity detector and two columns, a Molsieve 5A and a PoraPLOT Q. Analytical values were expressed as the conversions of CO and H<sub>2</sub>, and the yields of CO<sub>2</sub> and H<sub>2</sub>. The conversions were calculated from the ratio of the inlet and outlet molar flow rates as  $1 - F_{\text{outlet}}/F_{\text{inlet}}$ , where  $F$  stands for the molar flow rate of CO or H<sub>2</sub>. The yields were obtained from the ratio of the outlet molar flow rate of CO<sub>2</sub> or H<sub>2</sub> over the inlet molar flow rate of CO.

## 3. Results and Discussion

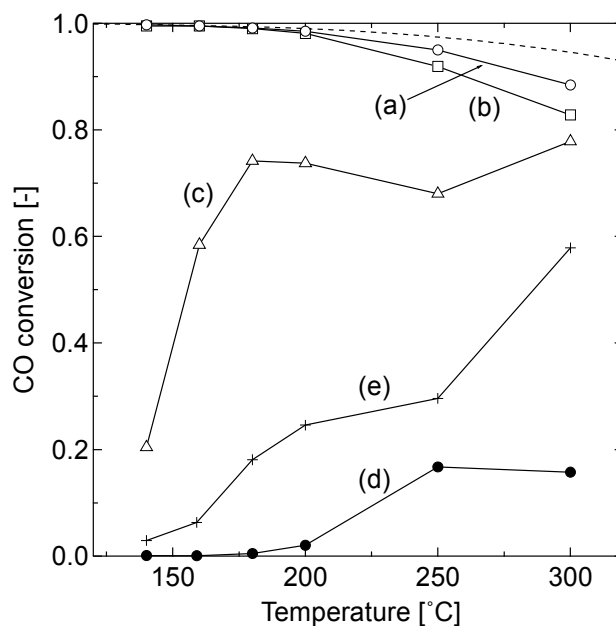
### 3.1. Temperature Dependence of Catalytic Activity in WGS

Figure 1 compares the catalytic activities of the prepared Au/Fe<sub>2</sub>O<sub>3</sub> catalysts in WGS. All of the samples were tested in the same temperature profile, wherein the temperature was raised at a rate of 10 °C min<sup>-1</sup> and maintained for 40 min at the given reaction temperature. An average value of conversion was calculated from three data collected during the last 10 min of the constant temperature period. Thermodynamically calculated equilibrium CO conversion curve is also drawn.

The CO conversions reached the equilibrium values below 200 °C in the samples loaded with 10 and 3 wt% Au and calcined at 200 °C. The CO conversion using these samples gradually decreased with increasing temperature and deviated from the equilibrium one because of a catalytic deactivation. In terms of the Au content, 3 wt% was enough to convert CO at low temperatures. However, the effect of Au content on CO conversion was significantly reduced at higher temperatures. The sample

calcined at 400 °C showed a lower activity at low temperatures, while the difference of conversion among the gold catalysts was reduced with the increase in reaction temperature.

**Figure 1.** Catalytic performance of Au/Fe<sub>2</sub>O<sub>3</sub> catalyst (as-prepared) in WGS (0.4 g catalyst, H<sub>2</sub>/CO/CO<sub>2</sub>/H<sub>2</sub>O = 45.9/8.3/4.1/41.7%, and GHSV = 2600 h<sup>-1</sup>); samples calcined at 200 °C with Au contents of (a) 10 wt%; (b) 3 wt%; (c) 1 wt%; (d) with no Au and (e) calcined at 400 °C with Au content of 3 wt%, and equilibrium CO conversion (dashed line).



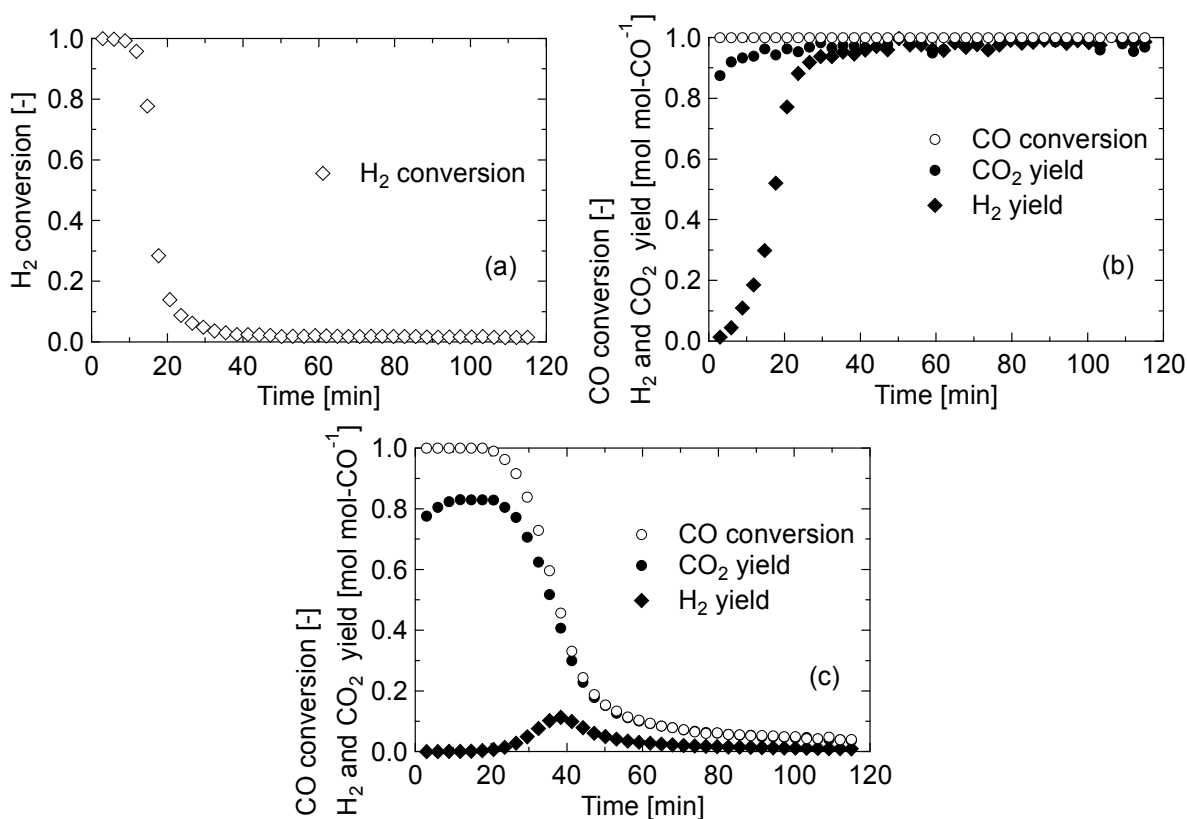
These results reflect the reaction system of WGS using an Au/iron oxide catalyst; the catalytic activity is caused by small Au particles activated by synergism with the support at low temperatures, gradually shifting to be support-dependent at high temperatures [20]. The catalytic activity of gold is diminished by the agglomeration of Au particles with the increase in reaction temperature. On the other hand, the reaction involves the reduction of Fe<sub>2</sub>O<sub>3</sub> to Fe<sub>3</sub>O<sub>4</sub> phase, which is a catalytically active oxidation state [19,20]. The shift in catalytic activity from Au-dependent to iron oxide dependent is clearly seen in the conversion curve of 1 wt% Au catalyst that showed low conversion of CO at 140 °C because of the low content of Au. The catalytic activity of Au increased with temperature up to 180 °C and then decreased due to the agglomeration, while the active site shifted to iron oxide at around 250 °C, leading to the increase in conversion at 300 °C.

The catalytic activity was thus affected by complicated structural change during the reaction. A temperature-programmed reduction (TPR) study of Au/iron oxide is well established, demonstrating that the reduction of iron oxide by H<sub>2</sub> at low temperature is accelerated by the existence of Au and by the lower crystallinity of iron oxide [22,23]. These studies suggest that the gold catalysts calcined at 200 °C of this study were activated to the form of Au/Fe<sub>3</sub>O<sub>4</sub> at the first test point of 140 °C. Namely, the control of the structure of Au/Fe<sub>3</sub>O<sub>4</sub> is essential to enhance the catalytic activity at low temperatures. In the following sections, we discussed the low-temperature pre-reduction for Au/Fe<sub>2</sub>O<sub>3</sub> catalyst (Au 3 wt%) calcined at 200 °C, which showed high catalytic activity, to develop more efficient catalyst for low-temperature WGS.

### 3.2. Pre-Reduction of Au/Fe<sub>2</sub>O<sub>3</sub> Calcined at 200 °C

The reduction temperatures employed were 140 and 200 °C. As reducing gases, CO and H<sub>2</sub> were used because they are possible reactants involved in WGS to reduce iron oxide, and CO/H<sub>2</sub>O was also used as a WGS condition. Using these conditions, the pre-reductions were conducted for 2 h, producing six kinds of reduced samples. The reduced catalysts were represented by reduction temperature and reducing gas, e.g., 140-CO.

**Figure 2.** Product gas during pre-reduction of Au/Fe<sub>2</sub>O<sub>3</sub> (3 wt% Au, calcined at 200 °C) as conversions of CO or H<sub>2</sub> and yields of CO<sub>2</sub> and H<sub>2</sub>; pre-reduction at 140 °C by (a) H<sub>2</sub>; (b) CO/H<sub>2</sub>O and (c) CO.



First, the reaction mechanism during the pre-reduction of Au/Fe<sub>2</sub>O<sub>3</sub> calcined at 200 °C was qualitatively discussed by analyzing the product gas. The produced gas was analyzed every 3 min during the treatment, and the conversions of CO or H<sub>2</sub> and the yields of H<sub>2</sub> and CO<sub>2</sub> were calculated. Figure 2 shows the change in the product gases for each treatment at 140 °C; (a) H<sub>2</sub> reduction, (b) CO/H<sub>2</sub>O reduction, and (c) CO reduction. In the pre-reduction treatments at 200 °C, similar results were obtained. The amounts of formed or consumed CO, H<sub>2</sub>, and CO<sub>2</sub> were calculated by integrating the conversions and yields, and summarized in Table 1. In H<sub>2</sub> pre-reduction treatment, the amount of H<sub>2</sub> consumed was nearly equal to the stoichiometrically calculated value, 1.91 mmol g-cat<sup>-1</sup>, based on the equation: Fe<sub>2</sub>O<sub>3</sub> + 1/3H<sub>2</sub> → 2/3Fe<sub>3</sub>O<sub>4</sub> + 1/3H<sub>2</sub>O. The reduction of iron oxide by H<sub>2</sub> is believed to progress through a dissociation of H<sub>2</sub> into hydrogen atoms on Au particles and the following spillover on iron oxide to drive the reduction as: Fe<sup>3+</sup>OH<sup>-</sup> + H → Fe<sup>2+</sup> + H<sub>2</sub>O [22]. In CO/H<sub>2</sub>O pre-reduction treatment, CO was completely consumed throughout the operating period, and CO<sub>2</sub> was maintained at

stoichiometric yield; however, it took about 40 min for H<sub>2</sub> to reach the stoichiometric yield. This result suggests that H<sub>2</sub> produced by WGS at the initial stage of the treatment was consumed for reducing iron oxide. The amount of H<sub>2</sub> consumed during CO/H<sub>2</sub>O pre-reduction was almost the same with that during H<sub>2</sub> pre-reduction. From these results, it was clarified that H<sub>2</sub> had a significant role to reduce iron oxide in the reduction. On the other hand, in CO pre-reduction treatment, the amount of CO consumed was about two-fold greater than the amount of H<sub>2</sub> consumed in other two pre-reductions, indicating that the CO pre-reduction cannot be represented simply by the equation, Fe<sub>2</sub>O<sub>3</sub> + 1/3CO → 2/3Fe<sub>3</sub>O<sub>4</sub> + 1/3CO<sub>2</sub>.

**Table 1.** Amounts of CO, H<sub>2</sub>, and CO<sub>2</sub> consumed and formed during pre-reduction.

Reducing gas	Temperature [°C]	Consumed [mmol g-cat <sup>-1</sup> ]		Formed [mmol g-cat <sup>-1</sup> ]	
		CO	H <sub>2</sub>	H <sub>2</sub>	CO <sub>2</sub>
H <sub>2</sub>	140	–	1.57	–	–
H <sub>2</sub>	200	–	1.67	–	–
CO/H <sub>2</sub> O <sup>a</sup>	140	–	1.62 <sup>b</sup>	–	–
CO/H <sub>2</sub> O <sup>a</sup>	200	–	1.73 <sup>b</sup>	–	–
CO	140	3.49	–	0.26	2.88
CO	200	3.41	–	0.23	2.64

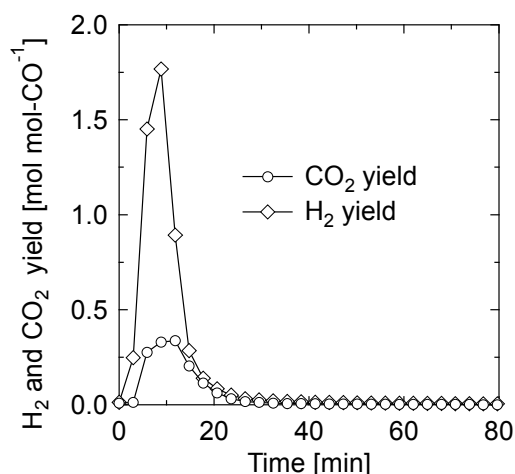
<sup>a</sup> Consumed CO, formed CO<sub>2</sub> and H<sub>2</sub> are not listed; <sup>b</sup> Calculated from H<sub>2</sub> yield assuming that H<sub>2</sub> was produced by WGS but consumed for the reduction of iron oxide.

Andreeva *et al.* [14] proposed the reaction mechanism of WGS on the Au/α-Fe<sub>2</sub>O<sub>3</sub> catalyst: the redox transfer cycle between Fe<sup>2+</sup> and Fe<sup>3+</sup> by ad/desorption of carbon species and the dissociative adsorption of H<sub>2</sub>O on Au particles. In this scheme, formate is formed from the adsorbed CO and the adjacent hydroxyl group, followed by desorption of CO<sub>2</sub> and H atom accompanying the reduction of Fe<sup>3+</sup> to Fe<sup>2+</sup> as: AuOH<sup>-</sup>Fe<sup>3+</sup> + CO → Au□Fe<sup>3+</sup>-COOH<sup>-</sup> → Au□Fe<sup>2+</sup> + CO<sub>2</sub> + H, where the symbol “□” expresses the site of iron oxide adjacent to Au, which presumably activates the Au for the dissociative adsorption of H<sub>2</sub>O.

Taking this scheme into consideration, an additional experiment was conducted for the CO-reduced sample as follows; the sample after 140-CO treatment was kept at the reduction temperature for 30 min under an Ar stream to completely purge CO, and then H<sub>2</sub>O with carrier Ar (H<sub>2</sub>O/Ar = 20/80) was introduced to the catalyst bed. Figure 3 shows the yield of product gas from the H<sub>2</sub>O introduction. H<sub>2</sub> began to form at the moment of H<sub>2</sub>O introduction, and the yield reached the maximum at 9 min and decreased to 0 within 40 min. Simultaneously, a small amount of CO<sub>2</sub> was formed. The amounts of H<sub>2</sub> and CO<sub>2</sub> formed through this operation were 1.34 and 0.38 mmol g-cat<sup>-1</sup>, respectively. This result confirms that the sample reduced by CO has a surprisingly active site for dissociative adsorption of H<sub>2</sub>O, expressed by the symbol “□”. The total amount of CO<sub>2</sub> formed through the successive treatment of CO reduction and H<sub>2</sub>O introduction was balanced with the amount of CO consumed in the reduction treatment. As for H<sub>2</sub>, the total amount was almost identical to the amount of H<sub>2</sub> consumed in H<sub>2</sub> pre-reduction and equal to half of that of CO<sub>2</sub> formed. Therefore, we can describe the scheme of the CO reduction treatment as: AuOFe<sup>3+</sup> + CO → Au□Fe<sup>2+</sup> + CO<sub>2</sub>. The following steam treatment involves the dissociative adsorption of H<sub>2</sub>O; therefore, the scheme is presumed as: Au□Fe<sup>2+</sup> + H<sub>2</sub>O → Au-H<sup>+</sup>OH<sup>-</sup>□Fe<sup>2+</sup> → AuOH<sup>-</sup>Fe<sup>3+</sup> + 1/2H<sub>2</sub>, thus leading to the initiation of the aforementioned WGS cycle.

The cause for the small amount of H<sub>2</sub> formed in the reduction treatment (Figure 2(c)) and CO<sub>2</sub> formed in the H<sub>2</sub>O treatment (Figure 3) cannot be specified, but minor reactions occurred by regional physical or chemical structure may account for this.

**Figure 3.** Yields of H<sub>2</sub> and CO<sub>2</sub> during H<sub>2</sub>O introduction to the catalyst reduced under 140-CO condition.



### 3.3. Characterizations of the Catalyst After Pre-Reduction

Analysis of the product gas from pre-reductions implied that iron oxide in the catalyst was reduced to Fe<sub>3</sub>O<sub>4</sub> phase even at 140 °C. Structural characteristics and XRD patterns of the reduced samples are shown in Table 2 and Figure 4, respectively. The BET surface area of the non-treated sample was about 200 m<sup>2</sup> g<sup>-1</sup>, with micropores having peak radius of 1.7 nm.

**Table 2.** Structural properties of the reduced samples.

Sample	$S_{\text{BET}}$ [m <sup>2</sup> g <sup>-1</sup> ]	Pore volume [mm <sup>3</sup> g <sup>-1</sup> ]	Pore peak radius [nm]	$D_{\text{Fe}_3\text{O}_4}$ <sup>a</sup> [nm]
140-CO	149	219	2.2	n/d <sup>b</sup>
200-CO	84	173	3.1	10.3
140-H <sub>2</sub>	87	196	4.2	10.1
200-H <sub>2</sub>	49	170	6.1	14.5
140-CO/H <sub>2</sub> O	68	224	6.1	11.4
200-CO/H <sub>2</sub> O	41	203	9.3	16.7

<sup>a</sup> Medium diameter of Fe<sub>3</sub>O<sub>4</sub> particles calculated from Fe<sub>3</sub>O<sub>4</sub> (220) peak at  $2\theta = 30.1^\circ$  based on Scherrer equation; <sup>b</sup> n/d means not detected.

The surface area significantly decreased with the increase in pore peak radius by the pre-reduction. The sample before the pre-reduction showed no distinct peaks in the XRD pattern (data not shown). On the other hand, XRD patterns of the reduced samples showed that the iron oxide was in the form of Fe<sub>3</sub>O<sub>4</sub>, although no peak appeared in the pattern of 140-CO. The ratio of intensities at the peaks of 30.1° and 35.5° (the most intense peak of magnetite),  $I_{30.1^\circ}/I_{35.5^\circ}$ , is 30 for pure Fe<sub>3</sub>O<sub>4</sub> [24]. When the crystallized iron oxide contains  $\alpha$ -Fe<sub>2</sub>O<sub>3</sub> phase, the intensity ratio decreases because  $\alpha$ -Fe<sub>2</sub>O<sub>3</sub> has the second most intense peak at 35.7° (overlapping with the most intense peak of magnetite) but does not

have in the vicinity of  $30.1^\circ$ . The  $I_{30.1^\circ}/I_{35.5^\circ}$  values of the reduced samples were between 28 and 35, with the exception of 140-CO that had undetectable crystallinity level. These results confirm that the majority of amorphous iron oxide was reduced to  $\text{Fe}_3\text{O}_4$  and crystallized during the pre-reduction. The highest level of crystallization occurred when  $\text{CO}/\text{H}_2\text{O}$  was used as reducing gas, followed by  $\text{H}_2$ . The reduction temperature also affected the crystallization and reduction ability. The surface area of the samples reduced at  $140^\circ\text{C}$  was about 1.7 times higher than that of the samples reduced at  $200^\circ\text{C}$  for all reducing gases. The reason for the different structure of 140-CO is still not clear, but is believed to be related to the oxidation state of iron oxide. In other words, the transformation to  $\text{Au}\square\text{Fe}^{2+}$  by CO pre-reduction has less impact on the structure of iron oxide, while the overall formation of  $\text{Fe}_3\text{O}_4$  phase by  $\text{H}_2\text{O}$  treatment can cause crystallization accompanied by decrease in surface area. In fact, when the 140-CO was treated with steam at  $80^\circ\text{C}$  for 40 min, the surface area decreased to  $71\text{ m}^2\text{ g}^{-1}$ .

**Figure 4.** XRD patterns of the reduced samples.

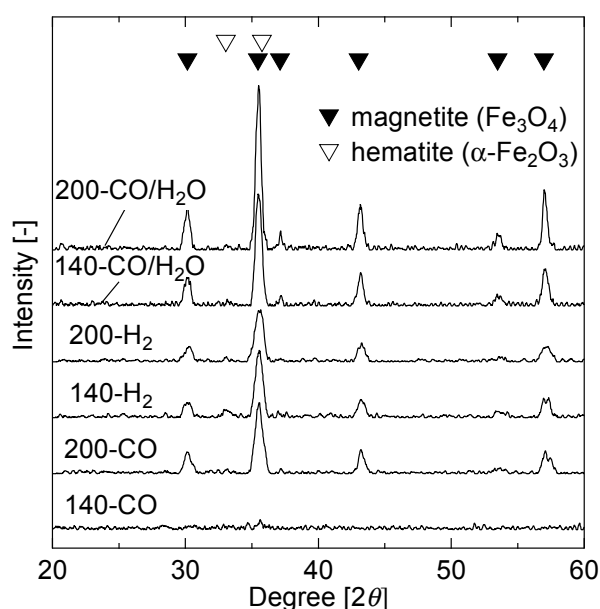
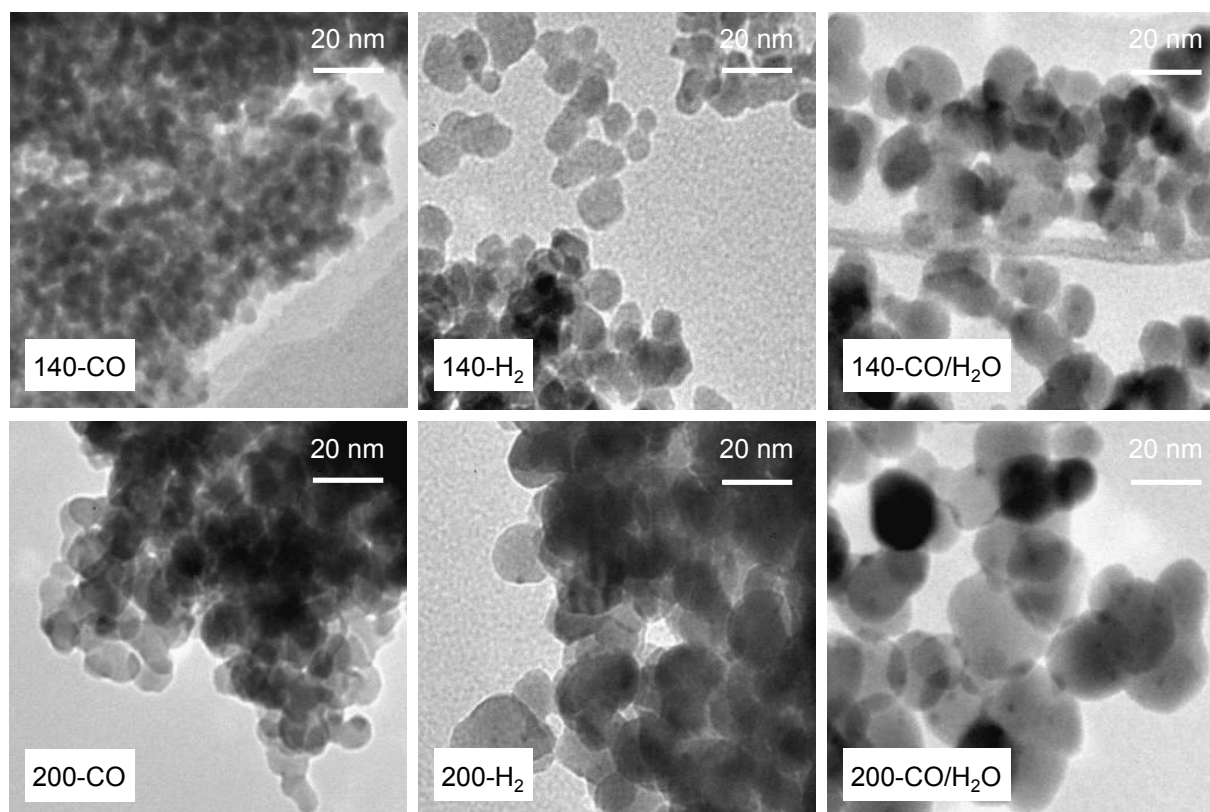


Figure 5 shows TEM photographs of the prepared  $\text{Au}/\text{Fe}_3\text{O}_4$  catalysts. The TEM observation confirms the difference between  $\text{Fe}_3\text{O}_4$  particles produced by each reduction treatment. The  $\text{Fe}_3\text{O}_4$  particles of 140-CO were less than 5 nm with their appearance being almost the same as that of the sample before pre-reduction, and the other catalyst also had small  $\text{Fe}_3\text{O}_4$  particles of about 20 nm. These particles of  $\text{Fe}_3\text{O}_4$  are surprisingly small compared to the direct synthesis of  $\text{Fe}_3\text{O}_4$  in liquid phase from  $\text{Fe}^{2+}/\text{Fe}^{3+}$  precursor by precipitation [25,26]. Most of the  $\text{Fe}_3\text{O}_4$  particles formed through the precipitation method are on a micrometer scale because the particle growth after the nucleation of  $\text{Fe}_3\text{O}_4$  by the dehydration reaction of  $\text{Fe}^{2+}$  and  $\text{Fe}^{3+}$  hydroxides cannot be controlled in the liquid phase synthesis. On the other hand, the formation of  $\text{Fe}_3\text{O}_4$  particles in this study progressed in the gas phase. The crystal growth in the gas phase can be thermally controlled, as obtained for the samples reduced at  $140^\circ\text{C}$  and  $200^\circ\text{C}$ . However, if the calcination temperature of  $\text{Au}/\text{Fe}_2\text{O}_3$  is the commonly-used  $400^\circ\text{C}$ , the formed  $\text{Fe}_3\text{O}_4$  particles would be large because the reduction of well-crystallized  $\text{Fe}_2\text{O}_3$  requires far higher temperatures. Moreover, when Au particles are not loaded on the iron oxide, the small  $\text{Fe}_3\text{O}_4$  particles would not be obtained because Au plays a role on decreasing the reduction

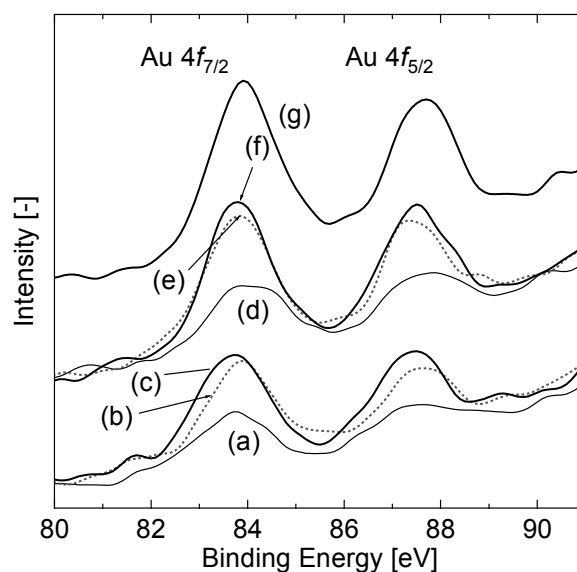
temperature [22,23]. Thus, the small  $\text{Fe}_3\text{O}_4$  particles were obtained only by reducing amorphous iron oxide loading of Au at low temperatures as proposed in this study, and the particle size was controllable with the reducing gas and reduction temperature.

**Figure 5.** TEM photographs of the reduced samples.



TEM photographs also showed Au particles having a diameter below 4 nm. However, it was difficult to identify the Au particles in 140-CO, 200-CO, and 140- $\text{H}_2$ . To investigate the state of Au loaded on the  $\text{Fe}_3\text{O}_4$  particles, XPS analysis was performed. Au 4f XPS spectra of the reduced samples are shown in Figure 6. Although the bulk Au shows a peak of Au 4f<sub>7/2</sub> electron binding energy of core levels at 84.0 eV, the value negatively shifts in general if it is a supported small nano-particle [27,28], as found at around 83.8 eV in this study. On the other hand, the binding energy of the cationic Au positively shifts by 0.8–1.4 and 2.8–3.5 eV for Au<sup>1+</sup> and Au<sup>3+</sup>, respectively [27–31]. These tendencies are applicable to Au 4f<sub>5/2</sub> having a peak at 88.0 eV for the bulk Au. These facts indicate that the partial existence of the cationic Au lowers the overall spectral intensity of Au 4f and gives shoulders at a binding energy above that of metallic Au [20]. The intensity of the spectrum in this study was varied among the reduced samples, and the differences showed a broad correlation with the structural characteristics of iron oxide. The sample 200-CO/ $\text{H}_2\text{O}$ , having the lowest surface area, showed the highest intensity; in contrast, the intensity of 140-CO was the lowest. This indicates that the crystallization and agglomeration of  $\text{Fe}_3\text{O}_4$  particles were accompanied by the reduction of the cationic Au, Au<sup>3+</sup> and Au<sup>1+</sup>, to metallic Au. Because the samples exhibiting a lower intensity of Au 4f peaks correspond to the samples having unobservable Au by TEM observation, the cationic Au was expected to be highly dispersed on the support in an undetectable state for the observation.

**Figure 6.** Au 4*f* spectra of the catalysts reduced at 140 °C by (a) CO; (b) H<sub>2</sub>; (c) CO/H<sub>2</sub>O, reduced at 200 °C by (d) CO; (e) H<sub>2</sub>; (f) CO/H<sub>2</sub>O and (g) 140-CO sample after 24 h of WGS at 80 °C.



#### 3.4. WGS at 80 °C Using Au/Fe<sub>3</sub>O<sub>4</sub> Catalysts

As shown in Figure 1, the Au/iron oxide catalyst calcined at 200 °C has sufficient catalytic activity to completely remove CO in the WGS at 140 °C. Therefore, we performed the WGS tests using the pre-reduced samples, namely Au/Fe<sub>3</sub>O<sub>4</sub> catalysts, at the low temperature of 80 °C to differentiate conversions of the samples and to determine whether the reaction progresses at such a low temperature. Prior to the tests, the reduced samples were purged under an Ar stream for 15 min at the reduction temperature, and the temperature was decreased to 80 °C, followed by H<sub>2</sub>O treatment for 40 min.

The performances of each Au/Fe<sub>3</sub>O<sub>4</sub> catalyst are shown in Figure 7 as CO conversion against reaction time for a period of 80 min. For all samples, stoichiometric amounts of H<sub>2</sub> and CO<sub>2</sub> were produced from H<sub>2</sub>O and CO during the reaction period. The pre-reduced catalysts were shown to be active for WGS even at 80 °C. Complete conversion was achieved by 140-CO and 140-H<sub>2</sub> during the majority of the reaction period, and 200-CO produced conversion above 0.9, corresponding to the reaction rate of  $2.3 \times 10^{-5}$  mol-CO g-Au<sup>-1</sup> s<sup>-1</sup> or more. Although the conversions using the other samples were above 0.6 at the initial stage of the reaction, they gradually decreased. From the characterization of Au/Fe<sub>3</sub>O<sub>4</sub> catalysts, the former and the latter groups were assigned to the reduced catalysts having surface areas greater and less than 80 m<sup>2</sup> g<sup>-1</sup>, respectively. The Au/Fe<sub>2</sub>O<sub>3</sub> catalyst calcined at 400 °C and preliminarily reduced by H<sub>2</sub> at 350 °C for 2 h was also examined for the 80 °C WGS reaction to compare the catalytic activity; however, it showed zero capability for CO conversion. These results elucidate our suggestion that the low-temperature pre-reduction of Au/Fe<sub>2</sub>O<sub>3</sub> catalyst having amorphous iron oxide to prepare Au/Fe<sub>3</sub>O<sub>4</sub> catalysts is very effective for low-temperature WGS reaction. Au/Fe<sub>3</sub>O<sub>4</sub> catalysts that were appropriately reduced before WGS showed a potential to completely remove CO even at the operating temperature of PEFC, 80 °C, which indicated that a compact on-site H<sub>2</sub> production system, where the CO oxidation section is not necessary, can be developed using the catalyst developed in this study.

**Figure 7.** WGS at 80 °C using Au/Fe<sub>3</sub>O<sub>4</sub> catalysts (0.3 g of catalyst, CO/H<sub>2</sub>O/N<sub>2</sub> = 2.2/30.3/67.5%, GHSV = 2800 h<sup>-1</sup>).

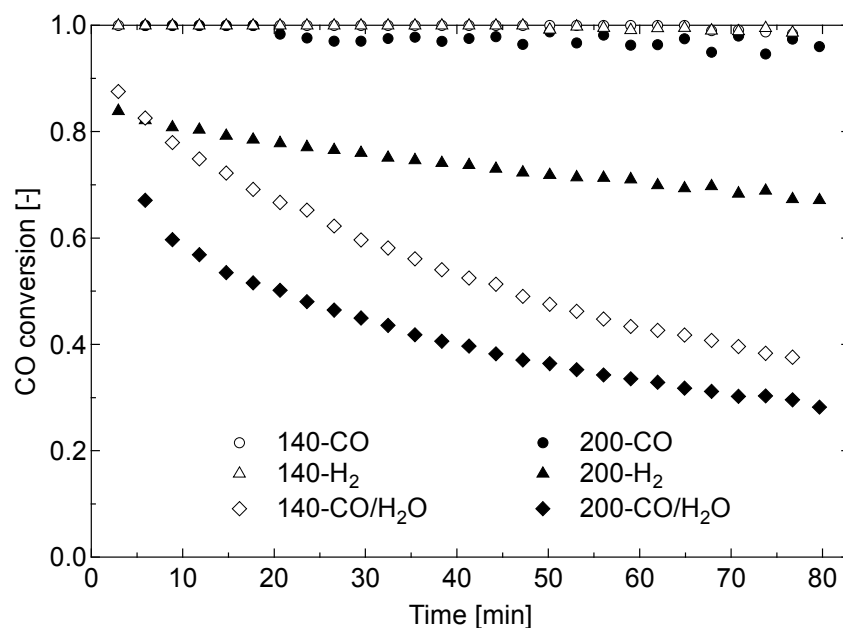
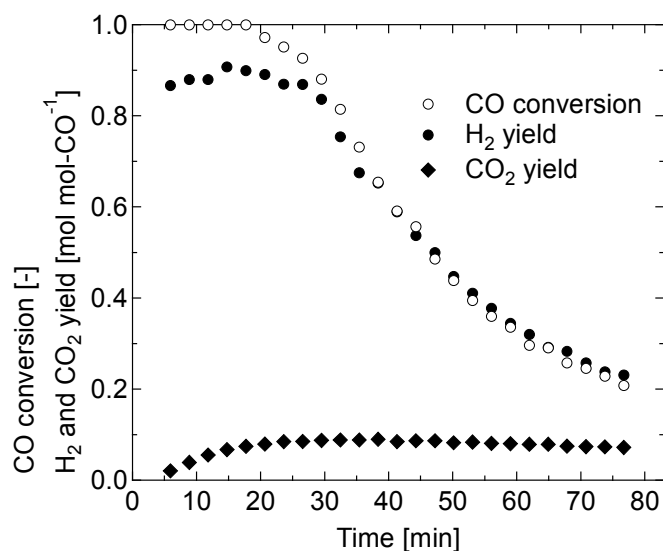


Figure 8 shows the result of 80 °C WGS using non-reduced Au/Fe<sub>2</sub>O<sub>3</sub> catalyst. Although high conversion was obtained at the initial stage of the reaction, appropriate amounts of H<sub>2</sub> were not produced, which is similar to the reaction behavior observed during CO pre-reduction (Figure 2(c)). This indicates that the WGS cycle, which is promoted by redox transfer between Fe<sup>2+</sup> and Fe<sup>3+</sup>, did not occur despite the presence of H<sub>2</sub>O in the reactant. CO conversion and CO<sub>2</sub> yield show that the reduction of iron oxide progressed, but the low yield of H<sub>2</sub> shows that the catalyst was inactive for dissociative adsorption of H<sub>2</sub>O. The reduction of iron oxide by CO was caused by high activity of Au nano-particles for adsorption of CO. In fact, Silberova *et al.* [32] found with DRIFTS study that the conversion of CO to CO<sub>2</sub> on Au/Fe<sub>2</sub>O<sub>3</sub> catalyst occurs even at a room temperature through the decomposition of the carbonate species. Meanwhile, low activity for the dissociative adsorption of H<sub>2</sub>O observed in this non-reduced catalyst shows that the site on iron oxide to activate Au for the reaction, “□”, was not formed. This is possibly due to a low crystallinity of the iron oxide support resulted from the low reaction temperature. In the case of Fe<sub>2</sub>O<sub>3</sub>-ZnO and Fe<sub>2</sub>O<sub>3</sub>-ZrO<sub>2</sub> catalysts, Au on the crystallized metal oxide was more active compared to the one on amorphous metal oxide for WGS [33]; therefore, it is believed that the site for dissociative adsorption of H<sub>2</sub>O cannot be formed on amorphous iron oxides. Similarly to CO oxidation using gold catalysts, where the rate-determining step is the activation of oxygen [34], it is important to activate the catalyst for the dissociative adsorption of H<sub>2</sub>O. The Au/iron oxide catalyst employed here, thus indicated, can have high catalytic activity for low-temperature WGS only when appropriately reduced and crystallized before the reaction.

**Figure 8.** Catalytic performance of non-reduced Au/Fe<sub>2</sub>O<sub>3</sub> (3 wt% Au, calcined at 200 °C) for WGS at 80 °C (0.3 g of catalyst, CO/H<sub>2</sub>O/N<sub>2</sub> = 2.2/30.3/67.5%, GHSV = 2800 h<sup>-1</sup>).



The catalytic activity of the samples, which showed high conversion during the 80 min reaction period, gradually decreased after further reaction time. The conversion of 140-CO after 24 h of 80 °C WGS was 0.21, with a decrease in surface area to 48 m<sup>2</sup> g<sup>-1</sup>. Possible factors for the catalytic deactivation are the formation of carbon species on the catalyst surface and degradation of the Au particles and of Fe<sub>3</sub>O<sub>4</sub>. Although there is small number of studies on the deactivation of the gold catalyst during WGS, Kim and Thompson [35] specified the deposition of formate and carbonate species on the catalyst surface to cause the deactivation in Au/CeO<sub>2</sub> catalyst. In our study, deconvolution of C 1s spectra in XPS analysis showed that the area proportion of –COOR:CO<sub>3</sub><sup>2-</sup> among R-OH (286.0 eV), –COOR:CO<sub>3</sub><sup>2-</sup> (288.5 eV), adventitious carbon (284.6 eV), and adsorbed CO<sub>2</sub> (undetected) species was 17.9/17.8% before/after 24 h of 80 °C WGS reaction, respectively, for the 140-CO sample. Additionally, the intensity of the –COOR:CO<sub>3</sub><sup>2-</sup> peak did not significantly change before and after the 24 h reaction. Thus, since there was little difference during the long-term reaction, the formation of carbon species cannot explain the catalytic deactivation. On the other hand, the increase in Au 4f spectrum intensity in XPS analysis was observed after 24 h of reaction (Figure 6(g)), which represents the transformation of cationic Au to the metallic state. As reported in literatures that the cationic Au is responsible for high catalytic activity of the gold catalyst [36,37], the degradation of Au can lead to a decrease of catalytic activity. Considering that Au is responsible for the catalytic activity at low-temperature WGS, which was shown in Figure 1, it is deemed that the deactivation was caused mainly by the loss of cationic Au. Crystallization of Fe<sub>3</sub>O<sub>4</sub> and the resulting decrease in surface area can also affect the catalytic activity. However, because the crystallization accompanied the transformation of cationic Au to the metallic state, maintaining lower crystallinity and/or higher surface area would prevent the transformation of cationic Au, leading to the maintenance of high catalytic activity. Hereafter the most important issue for this catalyst is to develop a method for the prevention of structural change during WGS reaction.

#### 4. Conclusions

Based on the result of the WGS using as-prepared Au/Fe<sub>2</sub>O<sub>3</sub> catalyst in the temperature range of 140–300 °C, the Au 3 wt% Au/Fe<sub>2</sub>O<sub>3</sub> catalyst calcined at 200 °C was reduced at low temperatures to prepare catalytically active Au/Fe<sub>3</sub>O<sub>4</sub> catalysts. It was confirmed by the product gas analysis during the pre-reduction treatment that the amorphous Fe<sub>2</sub>O<sub>3</sub> was reduced to Fe<sub>3</sub>O<sub>4</sub> using the reducing gases of CO, H<sub>2</sub>, or CO/H<sub>2</sub>O even at 140 °C. Quantitative analysis indicated that the reduction of Fe<sup>3+</sup> to Fe<sup>2+</sup> was progressed stoichiometrically by 1/2H<sub>2</sub> in CO/H<sub>2</sub>O and H<sub>2</sub> pre-reductions and by one mole of CO in CO pre-reduction. The introduction of steam following the CO pre-reduction clarified the presence of a site, which activates the Au particles for the dissociative adsorption of H<sub>2</sub>O, on iron oxide support. The reduced catalyst in this way had very small Fe<sub>3</sub>O<sub>4</sub> particles less than 20 nm in diameter. Among the reducing gases used, the highest reducing ability was shown by CO/H<sub>2</sub>O, and the second was by H<sub>2</sub>, judging from the surface area and the crystallinity of the reduced samples. The characteristics of both Fe<sub>3</sub>O<sub>4</sub> and Au on the support varied with reduction conditions, and the difference affected the catalytic performance in the WGS. In detail, the produced Au/Fe<sub>3</sub>O<sub>4</sub> catalyst with a higher surface area and Au particles in a more cationic state showed higher catalytic activity, resulting in the complete conversion of CO even at 80 °C. Considering a poor catalytic activity of non-reduced Au/Fe<sub>2</sub>O<sub>3</sub> catalyst, formation of a site to activate the Au for dissociative adsorption of H<sub>2</sub>O was necessary to progress low-temperature WGS. From these results, it was clarified that the preparation method of Au/Fe<sub>3</sub>O<sub>4</sub> catalysts proposed in this study is effective for the activation of the catalyst in low-temperature WGS, leading to the development of a compact on-site H<sub>2</sub> production system without CO oxidation section.

#### Acknowledgements

This work was supported by the Knowledge Cluster Initiative program (Kyoto Environmental Nanotechnology Cluster) of the Ministry of Education, Culture, Sports, Science, and Technology (MEXT) of the Japanese Government.

#### References

1. Song, C. Fuel processing for low-temperature and high-temperature fuel cells challenges, and opportunities for sustainable development in the 21st century. *Catal. Today* **2002**, *77*, 17–49.
2. Wee, J.-H.; Lee, K.-Y. Overview of the development of CO-tolerant anode electrocatalysts for proton-exchange membrane fuel cells. *J. Power Sources* **2006**, *157*, 128–135.
3. Tanaka, Y.; Utaka, R.; Kikuchi, R.; Sasaki, K.; Eguchi, K. CO removal from reformed fuel over Cu/ZnO/Al<sub>2</sub>O<sub>3</sub> catalysts prepared by impregnation and coprecipitation methods. *Appl. Catal. A Gen.* **2003**, *238*, 11–18.
4. Haruta, M.; Kageyama, H.; Kamijo, N.; Kobayashi, T.; Delannay, F. Fine structure of novel gold catalysts prepared by coprecipitation. *Stud. Surf. Sci. Catal.* **1989**, *44*, 33–42.
5. Haruta, M.; Yamada, N.; Kobayashi, T.; Iijima, S. Gold catalysts prepared by coprecipitation for low-temperature oxidation of hydrogen and of carbon monoxide. *J. Catal.* **1989**, *115*, 301–309.

6. Haruta, M.; Daté, M. Advances in the catalysis of Au nanoparticles. *Appl. Catal. A Gen.* **2001**, *222*, 427–437.
7. Haruta, M. Gold as a novel catalyst in the 21st century: Preparation, working mechanism and applications. *Gold Bull.* **2004**, *37*, 27–36.
8. Seker, E.; Gulari, E.; Hammerle, R.H.; Lambert, C.; Leerat, J.; Osuwan, S. NO reduction by urea under lean conditions over alumina supported catalysts. *Appl. Catal. A Gen.* **2002**, *226*, 183–192.
9. Uphade, B.S.; Yamada, Y.; Akita, T.; Nakamura, T.; Haruta, M. Synthesis and characterization of Ti-MCM-41 and vapor-phase epoxidation of propylene using H<sub>2</sub> and O<sub>2</sub> over Au/Ti-MCM-41. *Appl. Catal. A Gen.* **2001**, *215*, 137–148.
10. Nkosi, B.; Coville, N.J.; Hutchings, G.J.; Adams, M.D.; Friedl, J.; Wagner, F.E. Hydrochlorination of acetylene using gold catalysts: A study of catalyst deactivation. *J. Catal.* **1991**, *128*, 366–377.
11. Mul, G.; Zwijnenburg, A.; van der Linden, B.; Makkee, M.; Moulijn, J.A. Stability and selectivity of Au/TiO<sub>2</sub> and Au/TiO<sub>2</sub>/SiO<sub>2</sub> catalysts in propene epoxidation: An *in situ* FT-IR study. *J. Catal.* **2001**, *201*, 128–137.
12. Edwards, J.K.; Solsona, B.E.; Landon, P.; Carley, A.F.; Herzing, A.; Kiely, C.J.; Hutchings, G.J. Direct synthesis of hydrogen peroxide from H<sub>2</sub> and O<sub>2</sub> using TiO<sub>2</sub>-supported Au-Pd catalysts. *J. Catal.* **2005**, *236*, 69–79.
13. Kang, Y.-M.; Wan, B.-Z. Preparation of gold in Y-type zeolite for carbon monoxide oxidation. *Appl. Catal. A Gen.* **1995**, *128*, 53–60.
14. Andreeva, D.; Idakiev, V.; Tabakova, T.; Andreev, A.; Giovanoli, R. Low-temperature water-gas shift reaction on Au/ $\alpha$ -Fe<sub>2</sub>O<sub>3</sub> catalyst. *Appl. Catal. A Gen.* **1996**, *134*, 275–283.
15. Andreeva, D.; Tabakova, T.; Idakiev, V.; Christov, P.; Giovanoli, R. Au/ $\alpha$ -Fe<sub>2</sub>O<sub>3</sub> catalyst for water-gas shift reaction prepared by deposition-precipitation. *Appl. Catal. A Gen.* **1998**, *169*, 9–14.
16. Andreeva, D. Low temperature water gas shift over gold catalysts. *Gold Bull.* **2002**, *35*, 82–88.
17. Andreeva, D.; Idakiev, V.; Tabakova, T.; Ilieva, L.; Falaras, P.; Bourlinos, A.; Travlos, A. Low-temperature water-gas shift reaction over Au/CeO<sub>2</sub> catalysts. *Catal. Today* **2002**, *72*, 51–57.
18. Lei, Y.; Cant, N.W.; Trimm, D.L. The origin of rhodium promotion of Fe<sub>3</sub>O<sub>4</sub>-Cr<sub>2</sub>O<sub>3</sub> catalysts for the high-temperature water-gas shift reaction. *J. Catal.* **2006**, *239*, 227–236.
19. Munteanu, G.; Ilieva, L.; Andreeva, D. Kinetic parameters obtained from TPR data for  $\alpha$ -Fe<sub>2</sub>O<sub>3</sub> and Au/ $\alpha$ -Fe<sub>2</sub>O<sub>3</sub> systems. *Thermochim. Acta* **1997**, *291*, 171–177.
20. Hua, J.; Wei, K.; Zheng, Q.; Lin, X. Influence of calcination temperature on the structure and catalytic performance of Au/iron oxide catalysts for water-gas shift reaction. *Appl. Catal. A Gen.* **2004**, *259*, 121–130.
21. Kudo, S.; Maki, T.; Yamada, M.; Mae, K. A new preparation method of Au/ferric oxide catalyst for low temperature CO oxidation. *Chem. Eng. Sci.* **2010**, *65*, 214–219.
22. Ilieva, L.I.; Andreeva, D.H.; Andreev, A.A. TPR and TPD investigation of Au/ $\alpha$ -Fe<sub>2</sub>O<sub>3</sub>. *Thermochim. Acta* **1997**, *292*, 169–174.
23. Li, J.; Zhan, Y.; Lin, X.; Zheng, Q. Influence of calcination temperature on properties of Au/Fe<sub>2</sub>O<sub>3</sub> catalysts for low temperature water gas shift reaction. *Acta Phys. Chim. Sin.* **2008**, *24*, 932–938.
24. JCPDS International Centre for Diffraction Data. *Powder Diffraction File, Inorganic Compounds 1978*; JCPDS: Newtown Square, PA, USA, 1978.

25. Mizukoshi, Y.; Shuto, T.; Masahashi, N.; Tanabe, S. Preparation of superparamagnetic magnetite nanoparticles by reverse precipitation method: Contribution of sonochemically generated oxidants. *Ultrason. Sonochem.* **2009**, *16*, 525–531.
26. Tang, B.; Yuan, L.; Shi, T.; Yu, L.; Zhu, Y. Preparation of nano-sized magnetic particles from spent pickling liquors by ultrasonic-assisted chemical co-precipitation. *J. Hazard. Mater.* **2009**, *163*, 1173–1178.
27. Moulder, J.F.; Stickle, W.F.; Sobol, P.E.; Bomben, K.D. *Hand Book of X-Ray Photoelectron Spectroscopy*; Physical Electronics Inc.: Eden Prairie, MN, USA, 1995.
28. Radnik, J.; Mohr, C.; Claus, P. On the origin of binding energy shifts of core levels of supported gold nanoparticles and dependence of pretreatment and material synthesis. *Phys. Chem. Chem. Phys.* **2003**, *5*, 172–177.
29. Hutchings, G.J.; Hall, M.S.; Carley, A.F.; Landon, P.; Solsona, B.E.; Kiely, C.J.; Herzing, A.; Makkee, M.; Moulijn, J.A.; Overweg, A.; *et al.* Role of gold cations in the oxidation of carbon monoxide catalyzed by iron oxide-supported gold. *J. Catal.* **2006**, *242*, 71–81.
30. Fu, Q.; Saltsburg, H.; Flytzani-Stephanopoulos, M. Active nonmetallic Au and Pt species on ceria-based water-gas shift catalysts. *Science* **2003**, *301*, 935–938.
31. Li, J.; Zhan, Y.; Zhang, F.; Lin, X.; Zheng, Q. Au/Fe<sub>2</sub>O<sub>3</sub> water-gas shift catalyst prepared by modified deposition-precipitation method. *Chin. J. Catal.* **2008**, *29*, 346–350.
32. Silberova, B.A.A.; Mul, G.; Makkee, M.; Moulijn, J.A. DRIFTS study of the water-gas shift reaction over Au/Fe<sub>2</sub>O<sub>3</sub>. *J. Catal.* **2006**, *243*, 171–182.
33. Tabakova, T.; Idakiev, V.; Andreeva, D.; Mitov, I. Influence of the microscopic properties of the support on the catalytic activity of Au/ZnO, Au/ZrO<sub>2</sub>, Au/Fe<sub>2</sub>O<sub>3</sub>, Au/Fe<sub>2</sub>O<sub>3</sub>-ZnO, Au/Fe<sub>2</sub>O<sub>3</sub>-ZrO<sub>2</sub> catalysts for the WGS reaction. *Appl. Catal. A Gen.* **2000**, *202*, 91–97.
34. Scirè, S.; Crisafulli, C.; Minicò, S.; Condorelli, G.G.; di Mauro, A. Selective oxidation of CO in H<sub>2</sub>-rich stream over gold/iron oxide: An insight on the effect of catalyst pretreatment. *J. Mol. Catal. A Chem.* **2008**, *284*, 24–32.
35. Kim, C.H.; Thompson, L.T. Deactivation of Au/CeO<sub>x</sub> water gas shift catalysts. *J. Catal.* **2005**, *230*, 66–74.
36. Guzman, J.; Gates, B.C. Catalysis by supported gold: Correlation between catalytic activity for CO oxidation and oxidation states of gold. *J. Am. Chem. Soc.* **2004**, *126*, 2672–2673.
37. Herzing, A.A.; Kiely, C.J.; Carley, A.F.; Landon, P.; Hutchings, G.J. Identification of active gold nanoclusters on iron oxide supports for CO oxidation. *Science* **2008**, *321*, 1331–1335.